Supplementary Materials for

Temporal integration of mitogen history in mother cells controls proliferation of daughter cells

Mingwei Min*, Yao Rong, Chengzhe Tian, Sabrina L. Spencer*

*Corresponding author. Email: sabrina.spencer@colorado.edu (S.L.S.); min_mingwei@grmh-gdl.cn (M.M.)

Published 2 April 2020 on *Science* First Release
DOI: 10.1126/science.aay8241

This PDF file includes:

Other Supplementary Material for this manuscript includes the following:
(available at science.sciencemag.org/cgi/content/full/science.aay8241/DC1)

MDAR Reproducibility Checklist (.pdf)

Materials and Methods

Cell culture

MCF10A cells (ATCC Cat# CRL-10317, RRID:CVCL_0598) were maintained in DMEM/F12 (Gibco) supplemented with 5% (v/v) horse serum (Gibco), 20 ng/mL epidermal growth factor (EGF, Sigma-Aldrich), 0.5 mg/mL hydrocortisone (Sigma-Aldrich, St. Louis, MO), 100 ng/mL cholera toxin (Sigma-Aldrich), 10 μg/mL insulin (Thermo Fisher), and penicillin/streptomycin. In EGF withdrawal experiments, both EGF and horse serum were removed from the medium. RPE-hTERT cells were obtained from J. Mansfeld at Technische Universität Dresden and cultured in DMEM/F12 with 10% (v/v) fetal bovine serum (FBS), 1X Glutamax, and penicillin/streptomycin. For time-lapse imaging, phenol-red free DMEM/F12 (Gibco) was used. All cells were cultured at 37 ºC at 5% CO_2.

Stable cell lines

MCF10A cells with mCitrine knocked into the *CCND1* or *CDKN1A* gene locus were described previously (*9*, *10*). These cells also express H2B-mTurquoise for cell tracking and DHB-mCherry as a CDK2 activity sensor. To overexpress Fra1, a previously described MCF10A cell line expressing H2B-mTurquoise and DHB-mVenus (*6*) was transduced with lentivirus encoding Fra1-mCherry (wild type or S252D-S265D mutant (*27*)). RPE-hTERT cells expressing Cyclin D1-mVenus from its endogenous locus were received from J. Mansfeld (*19*) and transduced with H2B-mIFP lentivirus (*28*) for cell tracking and DHB-mCherry lentivirus to monitor CDK2 activity (*6*). Transduced cells were sorted by FACS on the fluorescent color(s) they carry to establish the cell line.

To overexpress Cyclin D1 in a tetracycline-inducible manner, TurboID-Cyclin D1 was integrated into the FRT site in plain RPE-hTERT Flp-In parental cells (received from J. Mansfeld (*19*)) using the Flp-In system (Thermo Fisher). Stable clones were selected using G418 (500 μg/mL). Individual clones were tested for Cyclin D1 overexpression and positive clones were pooled. Cyclin D1 expression was induced with 1 μg/mL tetracycline for 12 hr.

Inhibitors

Mek inhibitor, PD-0325091 (S1036, Selleckchem) at 100 nM; CDK4/6 inhibitor, palbociclib (Selleckchem, S1116) at 1 μM; Erk inhibitor, SCH772984 (S7101, Selleckchem) at 100 nM; mTor inhibitor, torin 1 (HY-13003, MedChem) at 250 nM; puromycin (InvivoGen, ant-pr-1) at 0.625 μg/mL, and cycloheximide (Enzo Life Science, ALX-380-269-G001) at 10 μg/mL in Fig. S8 for complete translation inhibition and at 0.5 μg/mL in Fig. S9 to reduce translation rate.

Antibodies

The following antibodies were used: anti-Cyclin D1 clone SP4 (Lab Vision Cat# RM-9104-S0, RRID:AB_149914) at 1:2000 for WB and 1:500 for IF; anti-Cyclin D2 (abcam, ab207604) at 1:1000; anti-Cyclin D3 (Santa Cruz Biotechnology Cat# sc-6283, RRID:AB_627355) at 1:1000; anti-phospho-Rb S807/811 (Cell Signaling Technology Cat# 8516, RRID: AB_11179075) at 1:1000; c-Myc (Cell Signaling Technology Cat# 5605, RRID:AB_1903938) at 1:1000 for WB and at 1:250 for IF; anti-Fos (Cell Signaling Technology Cat# 2250, RRID:AB_2247211) at 1:1000 for WB and at 1:6400 for IF; anti-Fra1 (Santa Cruz Biotechnology Cat# sc-28310, RRID:AB_627632) at 1:1000 for WB and at 1:200 for IF; anti-p27 (BD Biosciences Cat# 610241, RRID:AB_397636) at 1:1000 for WB and at 1:200 for IF; anti-β-Tubulin (Cell

Signaling Technology Cat# 86298, RRID:AB_2715541) at 1:2000; anti-GAPDH (Cell Signaling Technology Cat# 5174, RRID:AB_10622025) at 1:2000; anti-rabbit IgG, HRP-linked (Cell Signaling Technology Cat# 7074, RRID:AB_2099233) at 1:2000; anti-mouse IgG, HRP-linked (Cell Signaling Technology Cat# 7076, RRID:AB_330924) at 1:2000; Alexa Fluor-647 secondary antibody (Molecular Probes Cat# A-21245, RRID:AB_141775) at 1:500.

siRNA oligos

siRNA oligos were synthesized either by Dharmacon: *CCND1* (LU-003210-00-0002), *CCND2* (LU-003211-00-0002), *CCND3* (LU-003212-00-0002) and *CDKN1B* (LU-003472-00-0002), or by IDT: *MYC* (hs.Ri.MYC.13.2), *JUN* (hs.Ri.JUN.13.2), *FOSL1* (hs.Ri.FOSL1.13.2), *FOS* (hs.Ri.FOS.13.3), *ETS1* (hs.Ri.ETS1.13.2), Negative Control DsiRNA (51-01-14-04). siRNA transfection was carried out using DharmaFECT 1 (Dharmacon) following the manufacturer's instructions. Cells were lysed 24 or 48 h after transfection, unless stated otherwise, for western blot to determine the knockdown efficiency.

Live-cell imaging

Cells were plated on a 96-well plate (Cellvis P96-1.5H-N) coated with collagen (Advanced BioMatrix, #5015) at least 16 hr prior to the start of imaging and at a density such that cells were sub-confluent throughout the imaging period. Cells were imaged on a Nikon Inverted Microscope Eclipse Ti-E PFS (Nikon) with a Spectra X light engine (Lumencor), a 10X 0.45 NA objective and appropriate filter sets. Images were taken by a Zyla 5.5 sCMOS camera (Andor) or an ORCA-Flash 4.0 CMOS camera (Hamamatsu) at a frequency of 1 frame per 12 min. During the imaging, cells were kept in a humidified, 37 ºC chamber at 5% CO_2. Light exposure time for each image was: 10-20 ms for CFP, 200-300 ms for YFP, 50-80 ms for mCherry, 500-600 ms for mIFP. CFP and mIFP were excited at 50% lamp intensity and others were excited at 100% intensity. Two or four sites were imaged per well with their positions spaced apart so that the exposure area for each site did not overlap with other sites. For experiments involving drug treatments, cells were first imaged without drug for 4-20 hr; the movie was then paused and drugs were added by exchanging 50% of the media in each well with medium containing a 2X drug concentration. To wash off drugs, cells were washed thrice with warmed full-growth medium.

IF, RNA-FISH, and other fixed-cell staining

In experiments in which live-cell imaging was followed by immunofluorescence (IF) or RNA Fluorescence In Situ Hybridization (FISH), cells were fixed immediately after live-cell imaging by incubation in 4% paraformaldehyde for 15 min at room temperature. In O-propargyl-puromycin (OPP) and 5-ethynyl-2′-deoxyuridine (EdU) incorporation experiments, cells were incubated in medium containing 20 μM OPP for 24 min or medium containing 10 μM EdU for 15 min at the end of the live-cell imaging and then fixed and processed according to the manufacturer's instructions (Thermo Fisher C10458 and C10340).

For IF, cells were incubated with a blocking/permeabilization buffer (3% BSA, 0.1% Triton X-100) for 1 hr at room temperature. Primary antibody staining was carried out overnight at 4 °C in the blocking buffer and visualized using secondary antibodies conjugated to Alexa Fluor 647. *CCND1* RNA FISH (Thermo Fisher, VA6-16943) was carried out using the ViewRNA ISH Cell Assay kit (Thermo Fisher) following the manufacturer's instruction.

Image processing and cell tracking

Raw images were subtracted by dark noise and then divided by illumination bias. Dark noise was measured by a blank image taken with light source closed. Illumination bias of each fluorescent channel was estimated by averaged cell-free contour of all images in that channel.

Segmentation and tracking of MCF10A cells were performed using a published pipeline (*29*); code available at https://github.com/scappell/Cell_tracking. In brief, log-transformed H2B-mTurquoise images were convolved with a rotationally symmetric Laplacian of Gaussian filter and objects were defined as contiguous pixels exceeding a threshold filter score defined using Ostu's method (*30*).

To segment the whole cell in RNA-FISH and OPP experiments, a channel with whole-cell staining (CDK2 sensor or OPP) was first binarized into foreground (cells) and background using a threshold manually defined for each experiment. The foreground was further segmented using seed-based watershed with segmented nuclei as seeds.

Segmented cell nuclei were tracked by screening the nearest future neighbor. Between frames where the imaging plate was removed from and put back in the microscope (for example, for drug addition, drug wash off, and IF, FISH, and OPP stain after live-cell imaging), the plate jitter was calculated by registering images of the nucleus-stained channel and corrected prior to tracking. The background of each image was subtracted using top-hat filtering after illumination bias correction. Mean nuclear intensities were measured by averaging the background-subtracted pixel intensities in each nucleus as defined by a segmented nuclear mask. CDK2 activity was calculated as the ratio of cytoplasmic to nuclear median sensor fluorescence, with the cytoplasmic component measured in a 4-pixel wide cytoplasmic ring outside of the nuclear mask.

The RPE-hTERT cells were tracked using EllipTrack (*31*), a global-local cell-tracking method for hard-to-track cells (code available at https://github.com/tianchengzhe/elliptrack). Briefly, segmented nuclei were fit with ellipses, which were then tracked by maximizing the combined probabilities of all cell tracks throughout the movie using the Viterbi algorithm. Mitotic events were identified through morphological features pre- and post-chromosome segregation. The probability that two ellipses in two consecutive frames are linked was calculated as a function of morphological similarity and migration probability, the parameters of which were either inferred from training data or defined empirically.

Single-cell analysis

In live-cell experiments, each daughter cell was classified as $CDK2^{inc}$, $CDK2^{low}$ or $CDK2^{emerge}$. Unless stated otherwise, CDK2 activity in MCF10A cells was examined at 3 hr after anaphase: $CDK2^{inc}$ cells have CDK2 activity greater than 0.5 at 3 hr after anaphase that stays high until cell division; $CDK2^{low}$ cells have CDK2 activity less than 0.5 at 3 hr after anaphase that stays low for the rest of the movie; $CDK2^{emerge}$ cells have CDK2 activity less than 0.5 at 3 hr after anaphase but have CDK2 activity that rises later in the movie. Traces that end within 3 hr after anaphase were not classified. In RPE-hTERT cells, CDK2 activity was examined at 5 hr after anaphase with the same 0.5 threshold for the classification.

The $CDK2^{inc}$ and $CDK2^{low}$ states are molecularly distinct cellular states. $CDK2^{inc}$ cells are born committed to cell cycle with hyper-phosphorylated Rb, whereas $CDK2^{low}$ are born with hypo-phosphorylated Rb and are sensitive to mitogen availability and thus not yet committed to the cell cycle (*6*, *9*). Because Rb phosphorylation is bimodally distributed in newly born cells (*9*), we treat the $CDK2^{inc}$ and $CDK2^{low}$ states as binary. Passage through the $CDK2^{low}$ state has been

described as passage through a transient quiescence (*6, 8–10, 32–34*). CDK2^{emerge} cells are CDK2^{low} cells that emerge from this transient quiescence to later re-enter the cell cycle. While the cellular state is binary, the timing with which CDK2^{low} cells become CDK2^{emerge} cells is a continuum, as cells can make this switch at any point after entry into the CDK2^{low} state. For MCF10A cells, we chose CDK2 activity at 3 hr after anaphase as the cut-off to classify CDK2^{inc} cells because the dominant population (80%) of cells increases its CDK2 activity within 3 hr after anaphase (Fig. 1C, 1F). The same applies to the 5 hr cut-off in RPE-hTERT cells (Fig. S2E).

To interrogate cell cycle phase-dependent effects in live-cell experiments, traces were pooled based on the time of mitosis relative to the perturbation (drug addition or siRNA addition). For daughter-cell fate vs. perturbation-relative-to-anaphase plots, each data point was calculated from cells that underwent anaphase (marked by H2B) ± one frame (MCF10A), or ± two frames (RPE-hTERT), relative to the frame under consideration (a window of 36 min or 1 hr, respectively, centered at the indicated time point). A sliding window of one frame per time point is plotted, resulting in a time resolution of one data point per 12 minutes. These plots typically include 40-200 cells per well per data point. CDK2^{inc}, CDK2^{low} or CDK2^{emerge} fractions were calculated for each well and mean ± 95% confidence interval from 3-8 wells is plotted (Fig. 1E, 1G, 2A, 3A, 3D bottom, 3F, S2B-C, S2F-G, S3, S4D, S6A, S7C-E). A lack of overlap in the 95% confidence interval is equivalent to showing a statistically significant difference via *t*-test with a p value < 0.05.

In experiments where IF, FISH, or OPP stain is preceded by live-cell imaging of CDK2 activity, the intensity of the fixed-cell stain in each cell was matched back to the CDK2 traces to determine CDK2 status and time-since-anaphase of the cell at fixation (Fig. 2D-E, 3B, 3E, S1B-C, S4C, S6D-E). To reconstruct the dynamics of protein levels, mRNA levels, and translation rates, a moving average ± 95% confidence of all CDK2^{inc} cells in a 36-min window (typically including 20-100 cells per condition per time window) is plotted.

In experiments where protein level or CDK2 activity dynamics were recorded from live-cell imaging, subpopulations were selected as specified in figure legends (usually cells in a specific cell-cycle phase at the time of perturbation); unless stated otherwise, traces of fluorescence intensity were aligned to anaphase and means ± 95% confidence plotted. This analysis typically includes 100-2000 single-cell traces per condition (Fig. 2B-C, 3D top, 3G, S4B, S5B, S8, S9A-C).

In experiments where only fixed-cell information is shown, cells in a specific cell-cycle phase were identified using DNA content. The signal of interest is plotted as mean ± 95% confidence interval or density distribution of 5000+ cells per condition (Fig. 3C, S7A, S9E).

All experiments in the study have been independently performed at least twice.

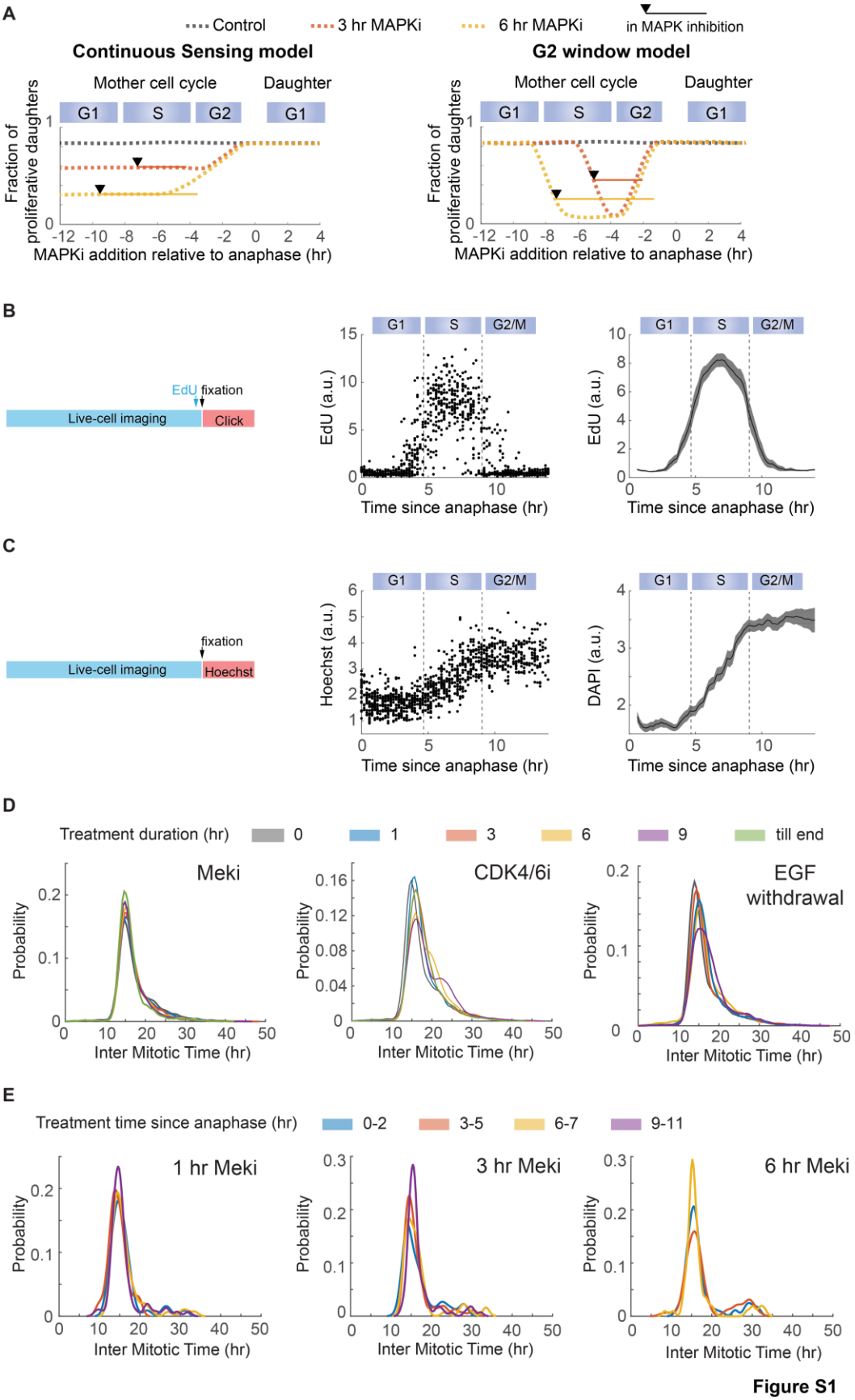
A
Control
3 hr MAPKi
6 hr MAPKi
in MAPK inhibition
Continuous Sensing model
G2 window model
Mother cell cycle
Daughter
G1
S
G2
Fraction of proliferative daughters
MAPKi addition relative to anaphase (hr)
B
EdU
fixation
Live-cell imaging
Click
G2/M
EdU (a.u.)
Time since anaphase (hr)
C
Hoechst
Hoechst (a.u.)
DAPI (a.u.)
D
Treatment duration (hr)
0
1
3
6
9
till end
Meki
CDK4/6i
EGF withdrawal
Probability
Inter Mitotic Time (hr)
E
Treatment time since anaphase (hr)
0-2
3-5
6-7
9-11
1 hr Meki
3 hr Meki
6 hr Meki

Figure S1

Fig. S1. Supporting data for testing the two mitogen sensing models.

(A) Decoupling the duration and cell-cycle phase of MAPK inhibition can differentiate between the two potential models: cells sense MAPK activity continuously throughout the mother cell cycle (left) or only in G2 phase (right). Each dot represents the fraction of proliferative daughters (y-axis) when a 3 hr or a 6 hr MAPKi treatment begins at the time indicated on the x-axis in mother cells. The solid horizontal lines show examples of treatment windows. (B) Establishing the timing of cell-cycle phases in asynchronously cycling MCF10A cells. Asynchronously cycling MCF10A cells expressing the CDK2 activity sensor and H2B-mTurquoise were imaged and tracked for 20 hr prior to a 15-min pulse of EdU and fixation. For each cell, time-since-anaphase was determined via time-lapse imaging and cell tracking of H2B-mTurquoise, and EdU incorporation was quantified via conjugation of Alexa 647 Azide using Click chemistry and visualization via fluorescent microscopy. EdU incorporation, a surrogate of DNA synthesis, is plotted as a function of time-since-anaphase for single cells (middle) and for population average (right, mean ± 95% confidence interval). (C) Same as **B** except that the total DNA content (rather than newly replicated DNA) was visualized by integrating the Hoechst signal in each nucleus. The two methods consistently show that on average, S phase in CDK2^{inc} MCF10A cells is from 4.5 hr to 9 hr after anaphase. (D) Probability density of inter-mitotic time in the ongoing cell cycle of MCF10A cells treated with Meki (left), CDK4/6i (middle) or EGF withdrawal (right) for various durations, showing that these perturbations do not change the length of the ongoing cell cycle. Cells with treatments initiated at any time during their cell cycle are included. (E) Probability density of inter-mitotic time in the ongoing cell cycle of MCF10A cells treated with Meki starting at different times since anaphase for 1 hr (left), 3 hr (middle) and 6 hr (right), showing that cells treated with Meki at different cell-cycle times do not differ in the length of the ongoing cell cycle. The color code indicates time of treatment initiation. Mitosis was marked by chromosome segregation visualized with H2B-mTurquoise.

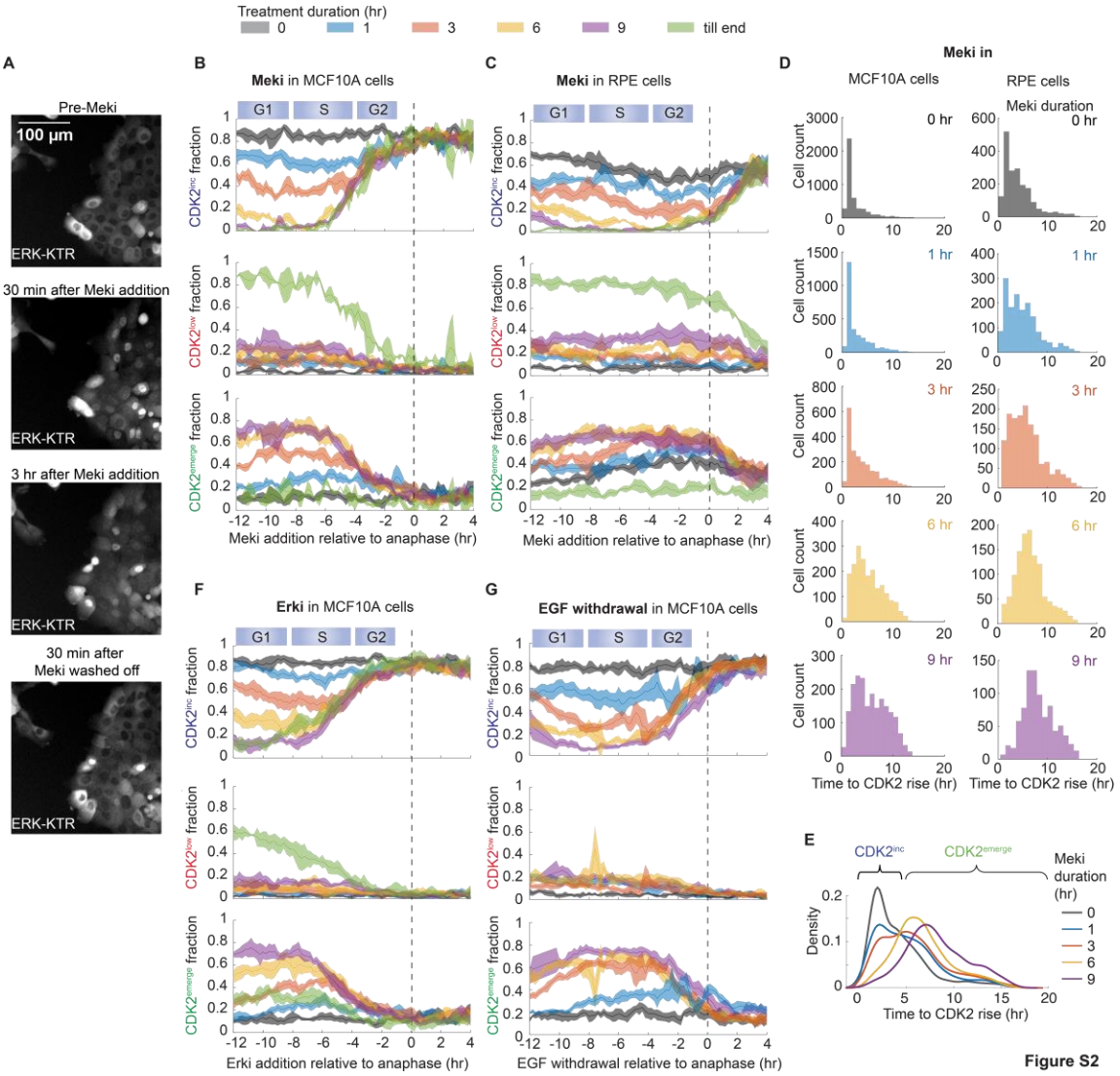

Fig. S2. Supporting data for the duration-dependent and cell-cycle phase-independent effect of Mek inhibition on cell proliferation.

(A) Images of an Erk activity sensor (ERK-KTR) (*35*, *36*) in MCF10A cells before and after Meki addition and wash-off. Nuclear signal indicates low Erk activity; cytoplasmic signal indicates high Erk activity. (B) Proliferation fate ($CDK2^{inc}$, $CDK2^{low}$ and $CDK2^{emerge}$ fraction) of MCF10A cells treated with Meki for 0, 1, 3, 6, or 9 hr, or till the end of the experiment, at various times relative to anaphase; data are plotted as mean fraction of $CDK2^{inc}$, $CDK2^{low}$, or $CDK2^{emerge}$ daughter cells with 95% confidence interval. The top panel is duplicated from Fig. 1E. (C) Proliferation fate of RPE-hTERT cells treated as in **B**. (D) Histogram of the time between anaphase and the rise of CDK2 activity in $CDK2^{inc}$ and $CDK2^{emerge}$ daughter cells in MCF10A (left) and RPE-hTERT (right). Cells were treated with Meki for the indicated durations starting from G1 phase of the mother cell cycle. (E) Density distribution of **D** for RPE-hTERT cells. (F) Proliferation fate of MCF10A cells treated with Erki for 0, 1, 3, 6, or 9 hr, or till the end of the experiment, at various times relative to anaphase; setup as in **B**. (G) Proliferation fate in which EGF was removed from MCF10A cells for 1, 3, 6, or 9 hr at various times relative to anaphase, and then put back.

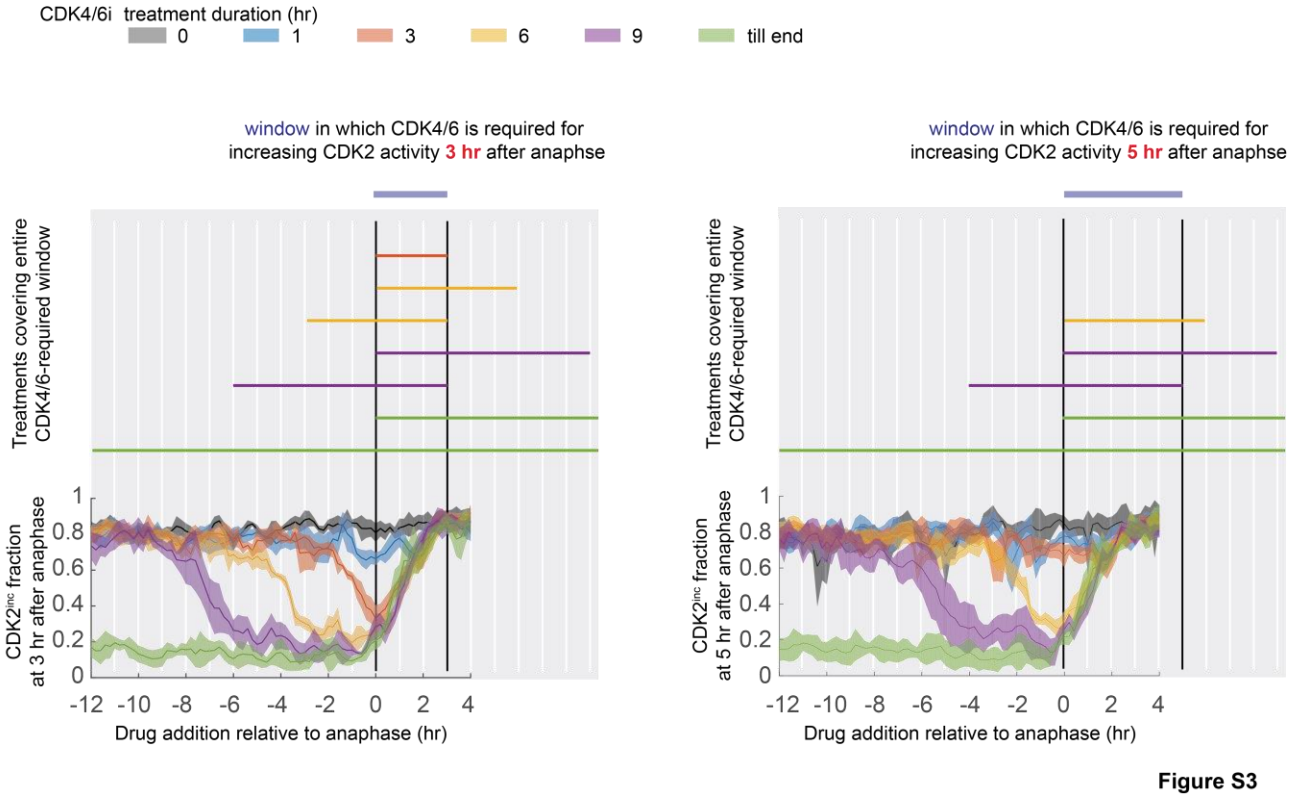

Figure S3

Fig. S3. Determination of CDK4/6i-sensitive window.

Left: Mean CDK2^{inc} fractions with 95% confidence interval plotted against the time of CDK4/6i addition. For a 3 hr CDK4/6i treatment, the treatment maximally inhibits proliferation when applied at anaphase, which inhibits CDK4/6 activity from 0 to 3 hr after anaphase (orange line). The 6 hr CDK4/6i treatment shows strongest proliferation reduction when begun any time between -3 and 0 hr relative to anaphase. Thus, the CDK4/6i-sensitive window can be derived from the intersection of these treatments (yellow lines), which is 0-3 hr after anaphase. Consistently, the CDK4/6i-sensitive window calculated from 9 hr CDK4/6i treatment also falls 0-3 hr after anaphase (purple lines). Thus, based on this analysis, cells are most sensitive to CDK4/6 inhibition between 0 and 3 hr after anaphase, marking a CDK4/6i-sensitive window. Right: Since 3 hr after anaphase is the time point that we classify CDK2^{inc} cells by examining the rise of CDK2 activity, CDK4/6 activity could either be required from 0 to 3 hr as a specific window in time, or could be required until the molecular event of the rise of CDK2 activity. To distinguish between these two ideas, cells were re-classified using a new scheme based on the CDK2 activity at 5 hr after anaphase. In this case, CDK4/6 inhibitor has to be present from 0 to 5 hr after anaphase to maximally inhibit the rise of CDK2 activity. Therefore, the window during which CDK4/6 activity is required for proliferation is dictated by the timing of CDK2 activity rise rather than by real time, and this window lasts from mitosis until after CDK2 activation.

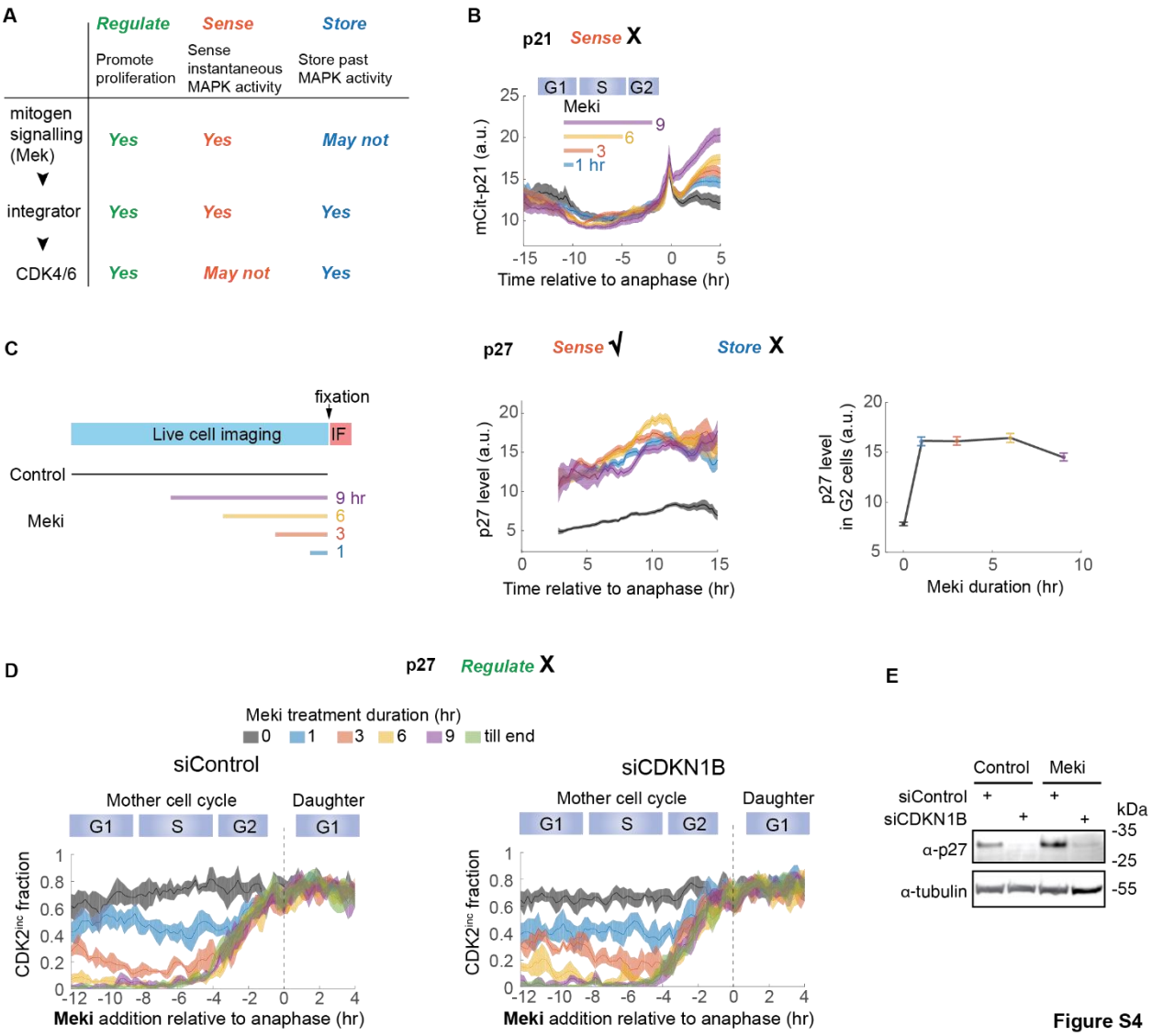

Figure S4

Fig. S4. Cell-cycle inhibitors p21 and p27 do not function as the integrator

(A) Expected properties of the MAPK integrator and its up- and down-stream regulators. (B) p21 is not rapidly induced by Meki treatment, but rather is only induced after the subsequent mitosis. Time-lapse imaging was carried out in MCF10A cells expressing mCitrine-p21 from its endogenous locus (*9*). Cells were treated with Meki for 0 (black curve), 1, 3, 6 or 9 hr; timing of treatment is indicated by the colored bars. Cells receiving Meki at the indicated window were grouped, traces were aligned to anaphase, and the mCitrine-p21 signal of each group is shown as mean ± 95% confidence interval. Since p21 levels do not change rapidly upon Meki addition, p21 does not actively sense MAPK activity [criterion (ii) not satisfied]. (C) p27 protein levels can sense Meki in all cell-cycle phases but do not record Meki duration. Time-lapse imaging of CDK2 activity in asynchronous cells was followed by fixation and staining with p27 antibody. Cells were treated with Meki for the indicated duration before fixation (left). The p27 intensity in $CDK2^{inc}$ cells was reconstructed as a function of time-since-anaphase and shown as mean ± 95% confidence interval; the black curve represents no Meki treatment (middle). Mean ± 95% confidence interval of p27 levels in G2 cells is plotted against the duration of Meki treatments

(right). G2 cells were identified as CDK2^{inc} cells at 10-12 hr after anaphase at the time of fixation with 4N DNA content. Since p27 levels do not reflect the Meki duration, p27 does not store Meki history [criterion (iii) not satisfied]. (D) Knockdown of p27 via siRNA does not alter cell fate in control or Meki treatment conditions. MCF10A cells expressing the CDK2 sensor were transfected with control siRNA or siRNA against CDKN1B gene (encoding p27) and imaged for 19 hr prior to Meki addition. Meki was then washed off after the indicated treatment duration and data were processed as in Fig. 1E. p27 knockdown does not restore proliferation of daughter cells in Meki conditions, indicating that upregulation of p27 is not responsible for Meki-induced quiescence. (E) Western blot of p27 to confirm knockdown. siRNA transfection and Meki addition were carried out in parallel to the experiments in **D**. Cells were lysed at 28 hr after siRNA transfection (9 hr after Meki addition).

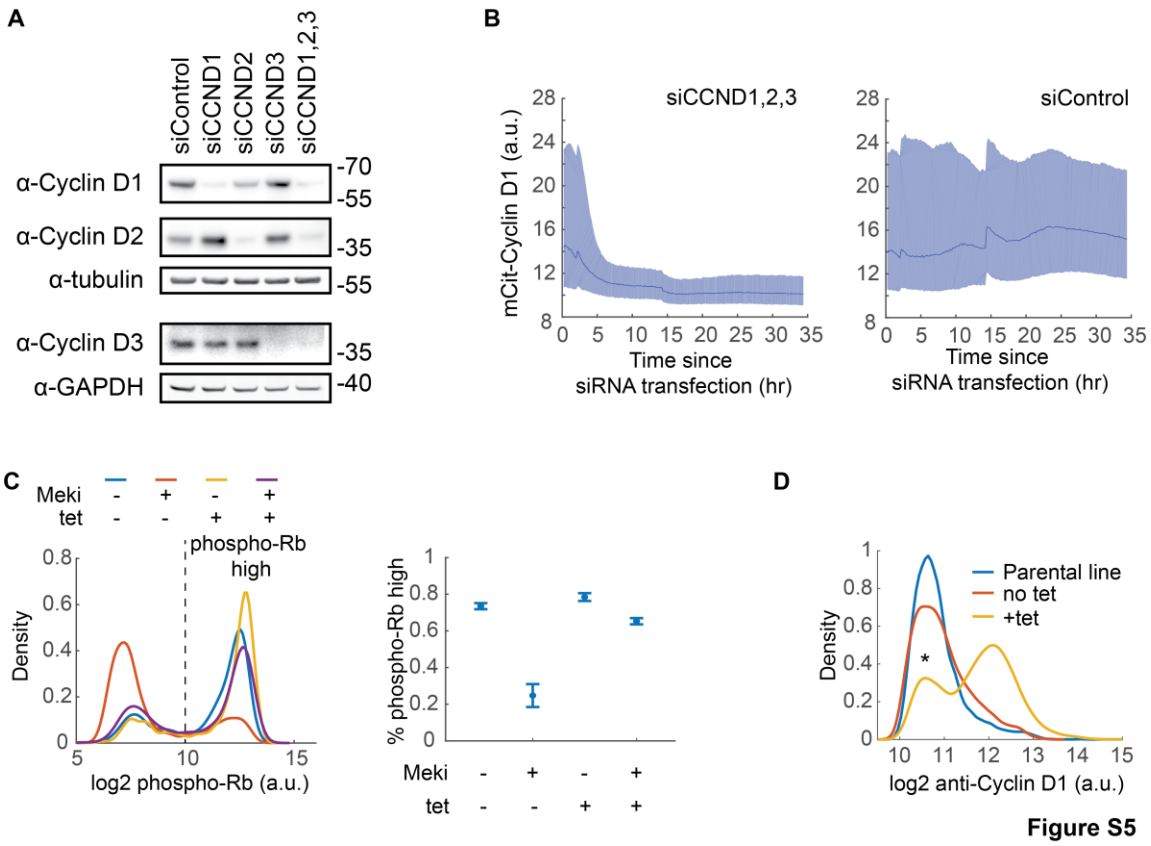

Fig. S5. Supporting data for Cyclin D's regulation of proliferation downstream of the MAPK pathway.

(A) Western blots of Cyclin D1, Cyclin D2 and Cyclin D3 for the indicated knockdown conditions. mCitrine-Cyclin D1 MCF10A cells were harvested at 24 hr after siRNA transfection. Tubulin and GAPDH are used as loading controls. (B) Live-cell imaging of mCitrine-Cyclin D1 levels in CCND knockdown and control conditions. Shaded areas indicate interquartile range and lines indicate median intensity in all nuclei. (C) Overexpression of Cyclin D1 can rescue the Meki-induced proliferation defect. TurboID-Cyclin D1 was expressed in a tetracycline-inducible RPE-hTERT cell line. Cells were treated with tetracycline together with Meki or DMSO for 12 hr before fixation, followed by phospho-Rb staining to determine the fraction of proliferating (phospho-Rb^{high}) vs. quiescent (phospho-Rb^{low}) cells. Only cells with 2N DNA content are included in the analysis. Left: the density distribution of phospho-Rb intensity of 3000+ single cells per condition. Right: mean ± 95% confidence interval of the phospho-Rb^{high} fraction across three wells. (D) Verification of Cyclin D1 overexpression. Cells were induced and fixed as in **C**, followed by staining with Cyclin D1 antibody. The density distribution of Cyclin D1 intensity is plotted for 3000+ 2N DNA content cells per condition. The asterisk indicates a small population of cells that has lost the Cyclin D1 expression construct and expresses endogenous level of Cyclin D1.

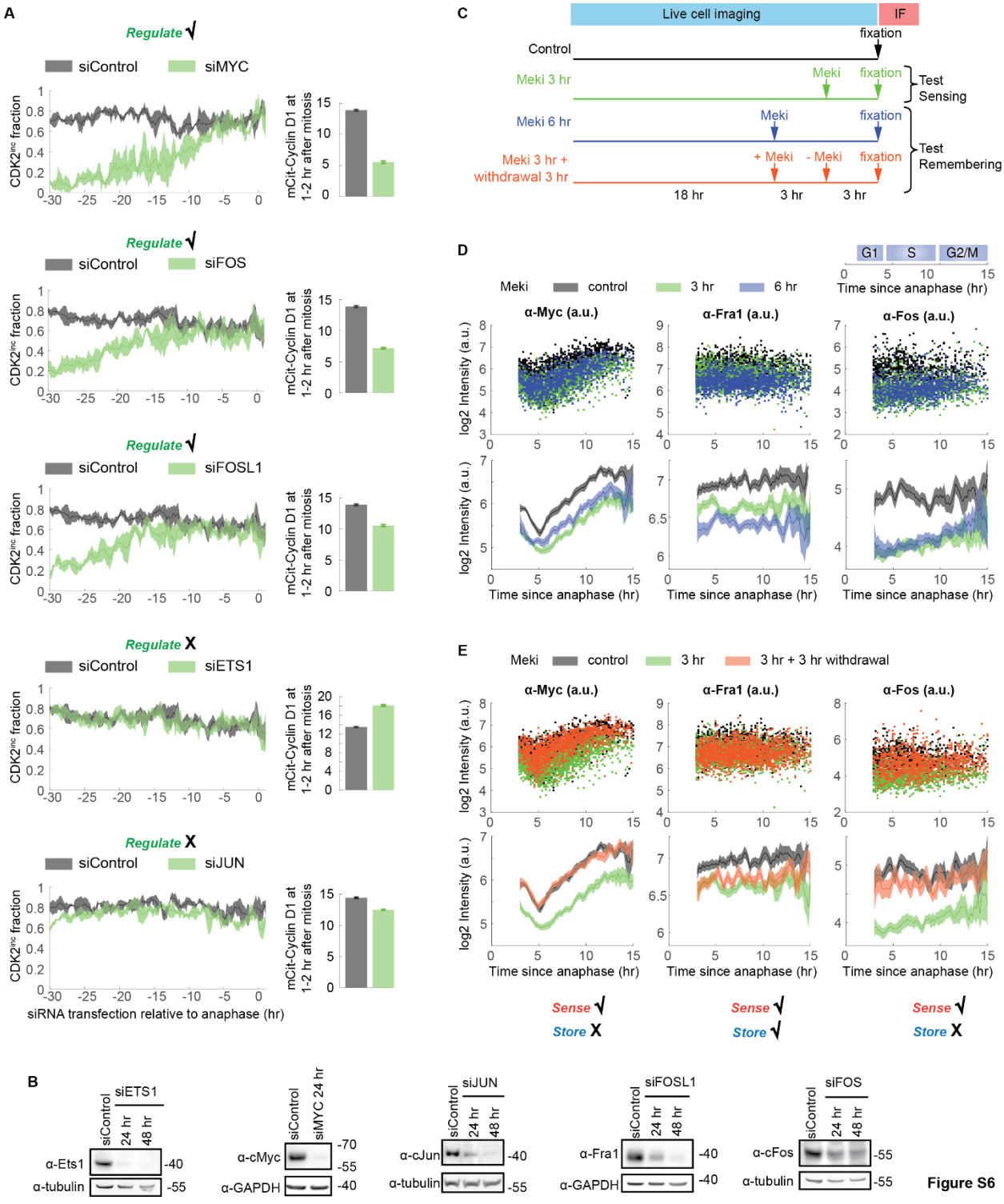

Fig. S6. Transcription factors for Cyclin D as potential integrators of MAPK signaling.

(A) Myc, Fos, and Fra1 (*FOSL1*) regulate cell proliferation in MCF10A cells. Cells were transfected with siRNA against the indicated transcription factors. Daughter-cell fates were monitored by time-lapse imaging of the CDK2 activity sensor and Cyclin D1 levels by the endogenous mCitrine tag. Left: Mean fractions of $CDK2^{inc}$ daughter cells with 95% confidence

interval are plotted against the time of siRNA transfection relative to anaphase. Right: Bar plots showing Cyclin D1 levels in early G1 daughter cells that underwent mitosis 20 hr post transfection (mean ± 95% confidence interval). (B) Western blots to verify knockdowns in **A**. Tubulin and GAPDH are used as loading controls. (C) Experimental scheme to test the capacity of Myc, Fos, and Fra1 to sense and store MAPK signaling. MCF10A cells were imaged for 24 hr to determine the cell-cycle phase of each cell. Cells were treated with Meki either for the final 6 hr of imaging, the final 3 hr of imaging, or for 3 hr followed by 3 hr release into full growth medium. Cells were then fixed and stained with antibodies against Myc, Fos, or Fra1. Immunofluorescence stains were matched to live-cell traces. Comparing 3 hr Meki at the end of the imaging to controls tests whether the levels of these transcription factors sense a short (3 hr) MAPK inhibition. Control vs. 3 hr Meki vs. 6 hr Meki tests whether cells can store the duration of Meki. A 3 hr Meki treatment at the end of the movie vs. 3 hr Meki + 3 hr release tests whether cells can carry memory of past Mek inhibition after a release. (D-E) Levels of Myc, Fos, and Fra1 protein were reconstructed as a function of time-since-anaphase in CDK2^{inc} cells. Top: each dot represents a single cell; bottom: moving average ± 95% confidence interval. The levels of all three transcription factors are able to sense Meki ("Sense") since their levels decrease after a 3-hr treatment (green in both D and E). However, Myc and Fos protein levels do not contain information on Meki duration, since their levels do not further reduce after a 6 hr Meki treatment compared to a 3 hr Meki treatment (D). Similarly, Myc and Fos levels do not store the past Meki treatment ("Store"), since their levels are restored to control levels 3 hr after Meki is washed off (E). Therefore, Myc and Fos levels are instantaneous MAPK sensors but are not MAPK integrators. By contrast, Fra1 levels encode the duration of Meki treatment and store past Meki treatment even after Meki is washed off. Therefore, Fra1 has properties of a MAPK activity integrator.

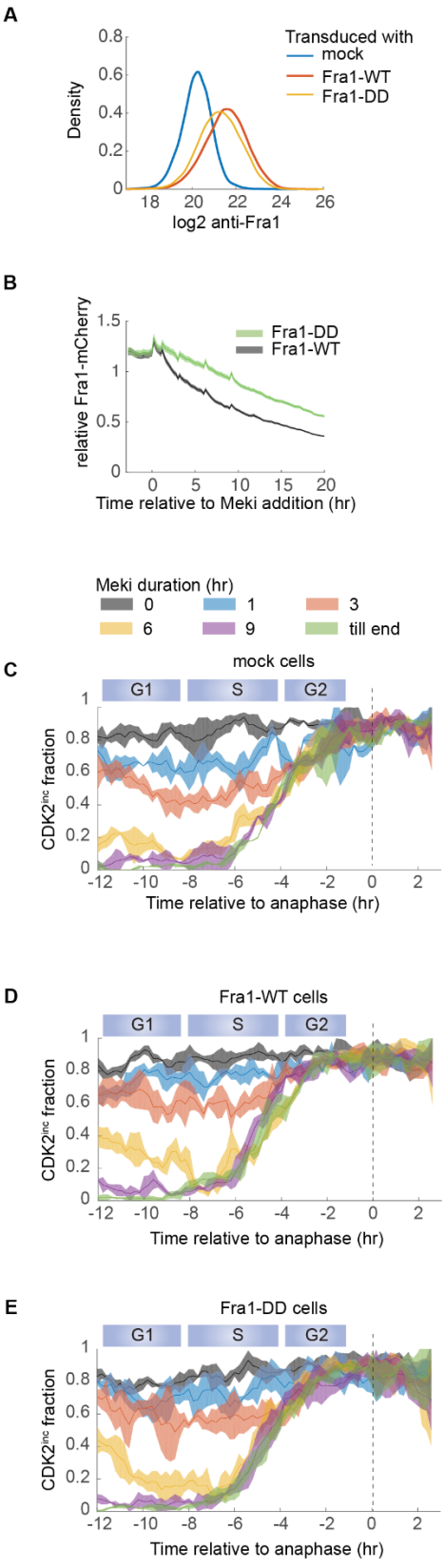

Figure S7

Fig. S7. Fra1 overexpression does not rescue the Meki-induced proliferation defect.

Erk regulates Fra1 at both the levels of transcription and protein stability, with the former at <3 hr time scale and the latter at a longer time scale (*12*). Thus, Fra1's integration property likely relies on protein stability. Two Erk-dependent phosphorylation sites have been implicated in promoting the stability of Fra1: S252 and S265 (*27*). We therefore constructed cell lines overexpressing wild type Fra1 (Fra1-WT) or phospho-mimetic Fra1 (Fra1-DD), and tested whether increasing the Fra1 levels (by reducing degradation) could override the Meki-induced proliferation defects. (A) Validation of Fra1 overexpression. Cells were fixed and stained with Fra1 antibody. Fra1 levels were quantified as total intensity in individual cells. (B) Fra1-DD mutant is degraded more slowly and thus is expressed at higher levels than Fra1-WT when Mek is inhibited. (C-E) Mean fraction of $CDK2^{inc}$ daughter cells with 95% confidence intervals in mock-transduced or Fra1-overexpressing cells treated with Meki at the indicated cell-cycle phase for the indicated durations. Fra1 overexpression (either WT or DD mutant) does not rescue the reduction of the $CDK2^{inc}$ fraction in Meki conditions.

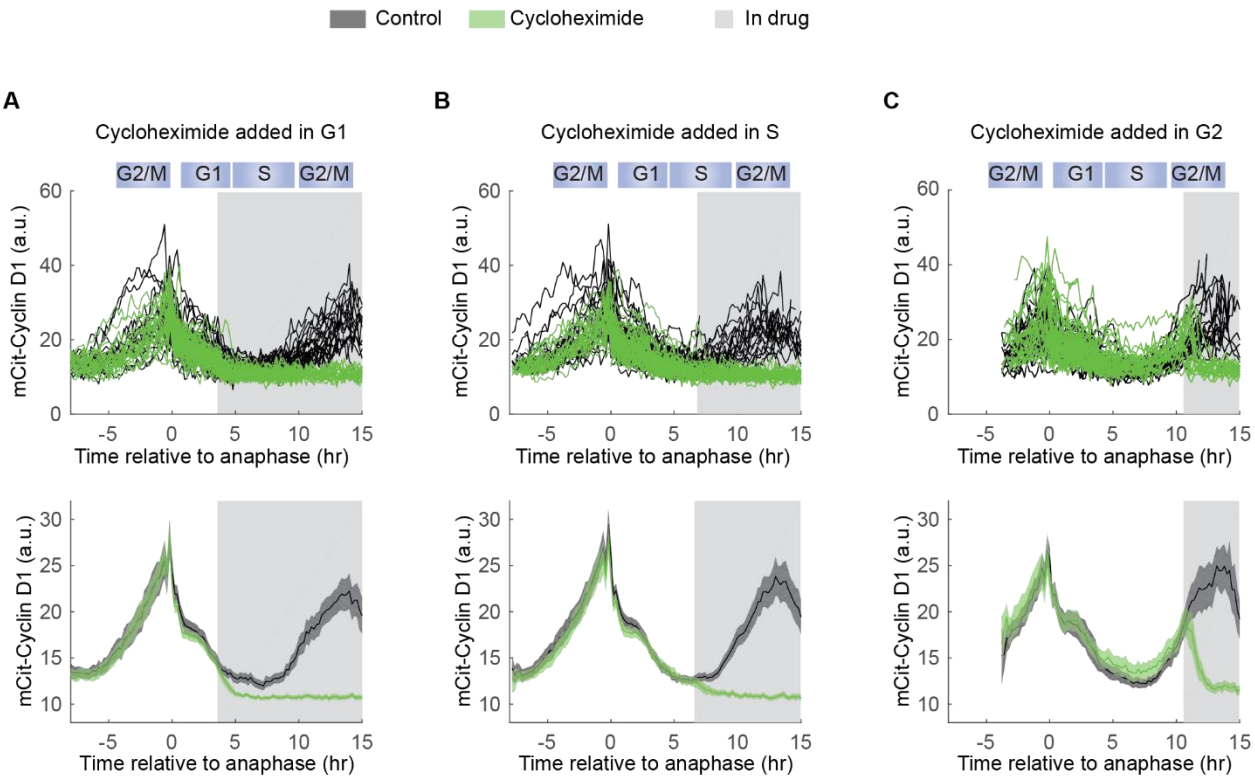

Figure S8

Fig. S8. Cyclin D1 is actively turned over in all cell-cycle phases.

Asynchronously cycling MCF10A cells expressing mCitrine-Cyclin D1 from its endogenous locus were imaged for 14 hr followed by treatment with translation inhibitor cycloheximide or equal volume of H_2O as a control. Top: Single-cell traces of cells receiving cycloheximide in G1 (A, $CDK2^{inc}$ cells at 3-4 hr after mitosis), S (B, $CDK2^{inc}$ cells at 6-7 hr after mitosis) or G2 (C, $CDK2^{inc}$ cells at 10-11 hr after mitosis) phase. Bottom: Mean ± 95% confidence interval of mCitrine-Cyclin D1 intensity for the conditions in **A**.

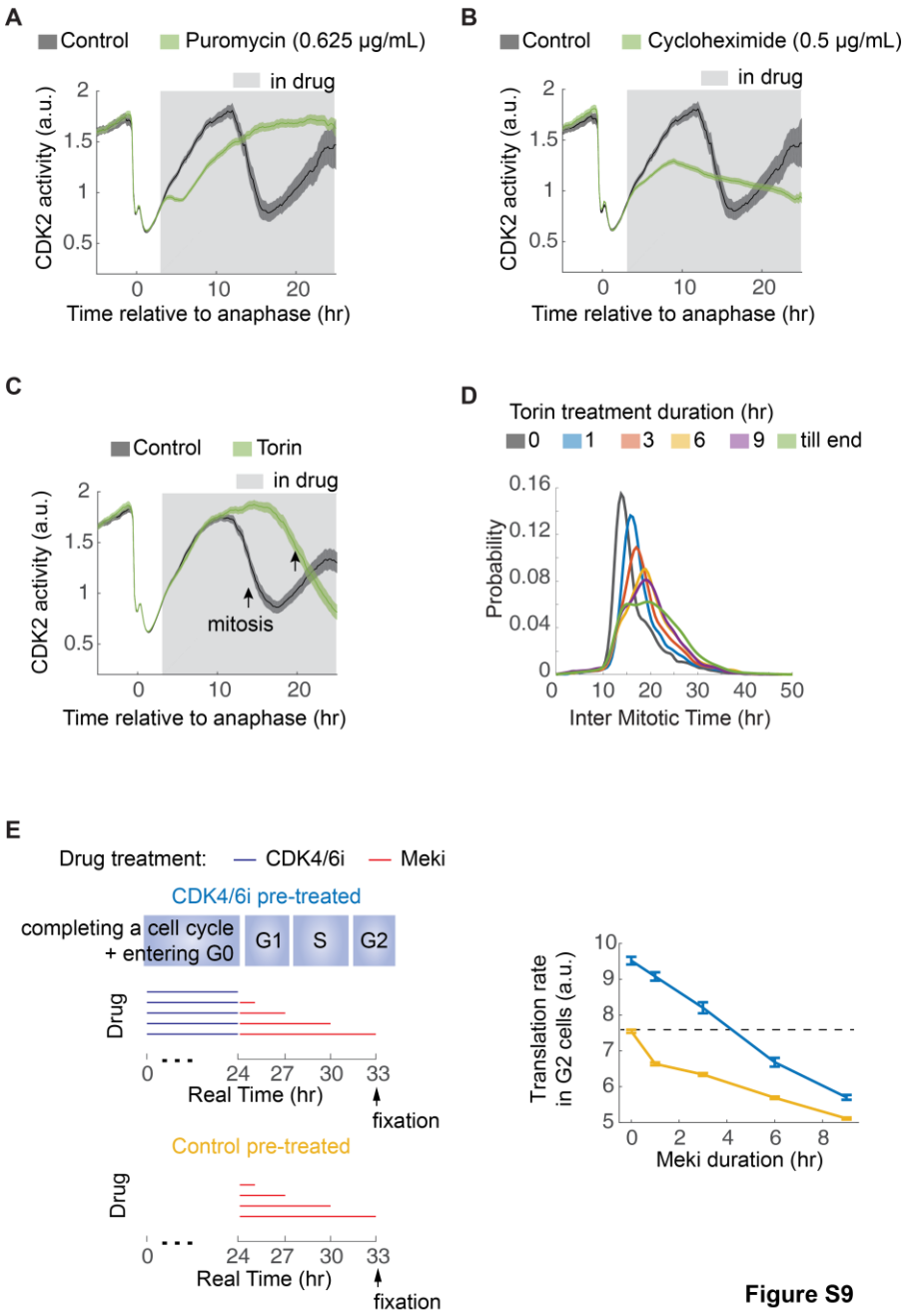

Fig. S9. Supporting data for global translation rate as the integrator.

(A-B) Direct perturbation of translation interferes with cell-cycle progression. Asynchronously cycling MCF10A cells expressing the CDK2 sensor were treated with puromycin (A) or cycloheximide (B). CDK2 traces of CDK2^{inc} cells receiving drug starting from mid-G1 were synchronized *in silico* to anaphase and plotted as mean ± 95% confidence interval. CDK2 activity plateaus or decreases upon addition of these translation inhibitors, indicating strong and immediate perturbation of ongoing cell cycle progression. (C) Same as in **A** and **B** except with mTor inhibitor torin. Unlike puromycin and cycloheximide, progression through the ongoing cell cycle (as read out by CDK2 activity) is not perturbed, but mitosis is delayed, as indicated by the arrows marking the time of mitosis. (D) Probability density of inter-mitotic time in the ongoing

cell cycle of MCF10A cells treated with torin for various durations. Mitosis was marked by chromosome segregation visualized with H2B-mTurquoise. These data were used to estimate the cell-cycle phase durations as a function of the duration of torin treatment, used in Fig. 3A. (E) CDK4/6i pre-treatment increases translation rate. Cells were treated with CDK4/6i (blue) or control (yellow) for 24 hr, followed by a 0, 1, 3, 6 or 9 hr Meki treatment. Cells were then pulsed with OPP and fixed. The amount of incorporated OPP was visualized via Click chemistry (25) and quantified as integrated intensity within each cell. Intensity distributions of OPP in G2 cells (identified by 4N DNA content) are compared. Dashed line depicts the translation rate in the unperturbed cells in normal growth conditions. In both control (yellow) and CDK4/6i pre-treated cells (blue), the translation rate decreases monotonically with longer Meki treatment. CDK4/6i enhances the baseline translation rate such that it rescues the reduction of translation induced by Meki (full rescue for $\leq$ 3 hr Meki and partial rescue for $\geq$ 6 hr Meki). The yellow curve is reproduced from Fig. 3C.

References and Notes

1. S. Meloche, J. Pouysségur, The ERK1/2 mitogen-activated protein kinase pathway as a master regulator of the G1- to S-phase transition. *Oncogene* **26**, 3227–3239 (2007). doi:10.1038/sj.onc.1210414 Medline

2. J. E. Toettcher, O. D. Weiner, W. A. Lim, Using optogenetics to interrogate the dynamic control of signal transmission by the Ras/Erk module. *Cell* **155**, 1422–1434 (2013). doi:10.1016/j.cell.2013.11.004 Medline

3. D. O. Morgan, *The Cell Cycle, Principles of Control* (New Science Press, 2007).

4. A. B. Pardee, A restriction point for control of normal animal cell proliferation. *Proc. Natl. Acad. Sci. U.S.A.* **71**, 1286–1290 (1974). doi:10.1073/pnas.71.4.1286 Medline

5. R. A. Weinberg, The retinoblastoma protein and cell cycle control. *Cell* **81**, 323–330 (1995). doi:10.1016/0092-8674(95)90385-2 Medline

6. S. L. Spencer, S. D. Cappell, F.-C. Tsai, K. W. Overton, C. L. Wang, T. Meyer, The proliferation-quiescence decision is controlled by a bifurcation in CDK2 activity at mitotic exit. *Cell* **155**, 369–383 (2013). doi:10.1016/j.cell.2013.08.062 Medline

7. M. Hitomi, D. W. Stacey, Cellular ras and cyclin D1 are required during different cell cycle periods in cycling NIH 3T3 cells. *Mol. Cell. Biol.* **19**, 4623–4632 (1999). doi:10.1128/MCB.19.7.4623 Medline

8. H. W. Yang, M. Chung, T. Kudo, T. Meyer, Competing memories of mitogen and p53 signalling control cell-cycle entry. *Nature* **549**, 404–408 (2017). doi:10.1038/nature23880 Medline

9. J. Moser, I. Miller, D. Carter, S. L. Spencer, Control of the Restriction Point by Rb and p21. *Proc. Natl. Acad. Sci. U.S.A.* **115**, E8219–E8227 (2018). doi:10.1073/pnas.1722446115 Medline

10. S. Gookin, M. Min, H. Phadke, M. Chung, J. Moser, I. Miller, D. Carter, S. L. Spencer, A map of protein dynamics during cell-cycle progression and cell-cycle exit. *PLOS Biol.* **15**, e2003268 (2017). doi:10.1371/journal.pbio.2003268 Medline

11. J. G. Albeck, G. B. Mills, J. S. Brugge, Frequency-modulated pulses of ERK activity transmit quantitative proliferation signals. *Mol. Cell* **49**, 249–261 (2013). doi:10.1016/j.molcel.2012.11.002 Medline

12. T. E. Gillies, M. Pargett, M. Minguet, A. E. Davies, J. G. Albeck, Linear Integration of ERK Activity Predominates over Persistence Detection in Fra-1 Regulation. *Cell Syst.* **5**, 549–563.e5 (2017). doi:10.1016/j.cels.2017.10.019 Medline

13. J. J. Liu, J. R. Chao, M. C. Jiang, S. Y. Ng, J. J. Yen, H. F. Yang-Yen, Ras transformation results in an elevated level of cyclin D1 and acceleration of G1 progression in NIH 3T3 cells. *Mol. Cell. Biol.* **15**, 3654–3663 (1995). doi:10.1128/MCB.15.7.3654 Medline

14. J. N. Lavoie, G. L'Allemain, A. Brunet, R. Müller, J. Pouysségur, Cyclin D1 expression is regulated positively by the p42/p44MAPK and negatively by the p38/HOGMAPK pathway. *J. Biol. Chem.* **271**, 20608–20616 (1996). doi:10.1074/jbc.271.34.20608 Medline

15. P. W. Hinds, S. Mittnacht, V. Dulic, A. Arnold, S. I. Reed, R. A. Weinberg, Regulation of retinoblastoma protein functions by ectopic expression of human cyclins. *Cell* **70**, 993–1006 (1992). doi:10.1016/0092-8674(92)90249-C Medline

16. S. A. Ezhevsky, H. Nagahara, A. M. Vocero-Akbani, D. R. Gius, M. C. Wei, S. F. Dowdy, Hypo-phosphorylation of the retinoblastoma protein (pRb) by cyclin D:Cdk4/6 complexes results in active pRb. *Proc. Natl. Acad. Sci. U.S.A.* **94**, 10699–10704 (1997). doi:10.1073/pnas.94.20.10699 Medline

17. C. J. Sherr, J. M. Roberts, Inhibitors of mammalian G1 cyclin-dependent kinases. *Genes Dev.* **9**, 1149–1163 (1995). doi:10.1101/gad.9.10.1149 Medline

18. M. Hitomi, D. W. Stacey, Cyclin D1 production in cycling cells depends on ras in a cell-cycle-specific manner. *Curr. Biol.* **9**, 1075–1084 (1999). doi:10.1016/S0960-9822(99)80476-X Medline

19. T. Zerjatke, I. A. Gak, D. Kirova, M. Fuhrmann, K. Daniel, M. Gonciarz, D. Müller, I. Glauche, J. Mansfeld, Quantitative Cell Cycle Analysis Based on an Endogenous All-in-One Reporter for Cell Tracking and Classification. *Cell Rep.* **19**, 1953–1966 (2017). doi:10.1016/j.celrep.2017.05.022 Medline

20. C. Albanese, J. Johnson, G. Watanabe, N. Eklund, D. Vu, A. Arnold, R. G. Pestell, Transforming $p21^{ras}$ mutants and c-Ets-2 activate the cyclin D1 promoter through distinguishable regions. *J. Biol. Chem.* **270**, 23589–23597 (1995). doi:10.1074/jbc.270.40.23589 Medline

21. P. M. Burch, Z. Yuan, A. Loonen, N. H. Heintz, An extracellular signal-regulated kinase 1- and 2-dependent program of chromatin trafficking of c-Fos and Fra-1 is required for cyclin D1 expression during cell cycle reentry. *Mol. Cell. Biol.* **24**, 4696–4709 (2004). doi:10.1128/MCB.24.11.4696-4709.2004 Medline

22. J. I. Daksis, R. Y. Lu, L. M. Facchini, W. W. Marhin, L. J. Penn, Myc induces cyclin D1 expression in the absence of de novo protein synthesis and links mitogen-stimulated signal transduction to the cell cycle. *Oncogene* **9**, 3635–3645 (1994). Medline

23. M. Polymenis, E. V. Schmidt, Coupling of cell division to cell growth by translational control of the G1 cyclin CLN3 in yeast. *Genes Dev.* **11**, 2522–2531 (1997). doi:10.1101/gad.11.19.2522 Medline

24. A. Litsios, D. H. E. W. Huberts, H. M. Terpstra, P. Guerra, A. Schmidt, K. Buczak, A. Papagiannakis, M. Rovetta, J. Hekelaar, G. Hubmann, M. Exterkate, A. Milias-Argeitis, M. Heinemann, Differential scaling between G1 protein production and cell size dynamics promotes commitment to the cell division cycle in budding yeast. *Nat. Cell Biol.* **21**, 1382–1392 (2019). doi:10.1038/s41556-019-0413-3 Medline

25. M. B. Ginzberg, N. Chang, H. D'Souza, N. Patel, R. Kafri, M. W. Kirschner, Cell size sensing in animal cells coordinates anabolic growth rates and cell cycle progression to maintain cell size uniformity. *eLife* **7**, e26957 (2018). doi:10.7554/eLife.26957 Medline

26. J. Liu, Y. Xu, D. Stoleru, A. Salic, Imaging protein synthesis in cells and tissues with an alkyne analog of puromycin. *Proc. Natl. Acad. Sci. U.S.A.* **109**, 413–418 (2012). doi:10.1073/pnas.1111561108 Medline

27. D. Yu, M. A. Baird, J. R. Allen, E. S. Howe, M. P. Klassen, A. Reade, K. Makhijani, Y. Song, S. Liu, Z. Murthy, S.-Q. Zhang, O. D. Weiner, T. B. Kornberg, Y.-N. Jan, M. W. Davidson, X. Shu, A naturally monomeric infrared fluorescent protein for protein labeling in vivo. *Nat. Methods* **12**, 763–765 (2015). doi:10.1038/nmeth.3447 Medline

28. J. Basbous, D. Chalbos, R. Hipskind, I. Jariel-Encontre, M. Piechaczyk, Ubiquitin-independent proteasomal degradation of Fra-1 is antagonized by Erk1/2 pathway-mediated phosphorylation of a unique C-terminal destabilizer. *Mol. Cell. Biol.* **27**, 3936–3950 (2007). doi:10.1128/MCB.01776-06 Medline

29. S. D. Cappell, M. Chung, A. Jaimovich, S. L. Spencer, T. Meyer, Irreversible APC(Cdh1) Inactivation Underlies the Point of No Return for Cell-Cycle Entry. *Cell* **166**, 167–180 (2016). doi:10.1016/j.cell.2016.05.077 Medline

30. N. Otsu, A Threshold Selection Method from Gray-Level Histograms. *IEEE Trans. Syst. Man Cybern.* **9**, 62–66 (1979). doi:10.1109/TSMC.1979.4310076

31. C. Tian, C. Yang, S. L. Spencer, EllipTrack: A Global-Local Cell-Tracking Pipeline for 2D Fluorescence Time-Lapse Microscopy. bioRxiv 2020.04.13.036756 [Preprint]. 13 April 2020. https://doi.org/10.1101/2020.04.13.036756.

32. H. M. Feldman, C. M. Toledo, S. Arora, P. Hoellerbauer, P. Corrin, L. Carter, M. Kufeld, H. Bolouri, R. Basom, J. Delrow, J. Meier, F. Zhang, J. L. McFaline-Figueroa, C. Trapnell, S. M. Pollard, C. L. Plaisier, P. J. Paddison, CRISPR-Cas9 Screens Reveal Genes Regulating a G0-like State in Human Neural Progenitors. bioRxiv 446344 [Preprint]. 17 October 2018. https://doi.org/10.1101/446344.

33. L. Krenning, J. van den Berg, R. H. Medema, Life or Death after a Break: What Determines the Choice? *Mol. Cell* **76**, 346–358 (2019). doi:10.1016/j.molcel.2019.08.023 Medline

34. G. Yao, Modelling mammalian cellular quiescence. *Interface Focus* **4**, 20130074 (2014). doi:10.1098/rsfs.2013.0074 Medline

35. S. Regot, J. J. Hughey, B. T. Bajar, S. Carrasco, M. W. Covert, High-sensitivity measurements of multiple kinase activities in live single cells. *Cell* **157**, 1724–1734 (2014). doi:10.1016/j.cell.2014.04.039 Medline

36. B. Sparta, M. Pargett, M. Minguet, K. Distor, G. Bell, J. G. Albeck, Receptor Level Mechanisms Are Required for Epidermal Growth Factor (EGF)-stimulated Extracellular Signal-regulated Kinase (ERK) Activity Pulses. *J. Biol. Chem.* **290**, 24784–24792 (2015). doi:10.1074/jbc.M115.662247 Medline